SPIE Astronomical Telescopes and Instrumentation
Vol. 5490, Glasgow, Scotland, June, 2004.

Tomography for multiconjugate adaptive optics systems using laser guide stars

Donald Gavel
UCO/Lick Observatory, University of California, Santa Cruz, California 95064

ABSTRACT

In this paper we present a solution to the MCAO reconstruction problem using multiple laser guide stars and show that it can be interpreted as a form of back-projection tomography. It is shown that a key intermediate step is to determine a minimum-variance estimate of the index variations over the atmospheric volume. We follow the idea of Tokovinin and Viard [JOSA-A, April 2001] in initially formulating the problem in the Fourier domain; we then extend the interpretation to the spatial domain. The former results were limited to the case of infinite aperture and plane wave beacons, and the statistically optimal wavefront solution was given for a single science direction. The new approach is more general and interpretable as tomographic back-projections, which gives rise to algorithms for the finite aperture, cone (laser) beams, and wide-science-field cases. A fortuitous consequence of this analysis is that a "fast" algorithm suitable for real-time implementation has become evident. The reconstruction requires only filtering and the inversion of small (dimension = number of guidestars) matrices. In simulations, we compare results with those of a spatial domain least-square matrix-inversion method.

Keywords: Adaptive Optics, Laser Guide Stars, Tomography Algorithms

1. INTRODUCTION

Multi-conjugate adaptive optics is currently an important area of research within the adaptive optics community, which is preparing to design systems for the next generation of giant telescopes. Several giant astronomical telescopes are now in their concept stages, with 20, 30, 50, even 100 meters diameter apertures proposed. The push toward large aperture telescopes, as well as the fact that astronomers wish to expand on the traditionally narrow adaptive optics field of view, has led to a need for multi-conjugate wavefront correction. Multi-conjugate adaptive optics involves the placement of several deformable mirrors in the AO system at optical conjugates to various turbulent layer heights in the atmosphere. If the turbulence is corrected at the altitudes at which it originates, then the accuracy of the correction is extended over larger field angles. For laser guide stars, the finite telescope aperture implies that the laser beacon rays will only probe a cone volume above the telescope, leaving increasing areas of turbulence unmeasured at higher altitudes. Multiple laser guidestar beacons at different field positions fill in the probed volume thus large telescope designs call for the use of multiple laser projectors. Lasers are preferred because the chance of finding a sufficiently bright natural guidestar beacon (or cluster of guidestar beacons for wide field) is statistically very small on the sky.

The problem of determining the commands to the multiple deformable mirrors given the measurements from multiple beacons is not a trivial one. In the many examples of adaptive optics systems implemented to date which only use one deformable mirror, conjugate to zero altitude, and one guidestar beacon, the approach is, at least conceptually, straightforward. The measured wavefront is inverted and placed on the deformable mirror. If slope sensors such as a Hartmann sensor, are used (as in the majority of cases) then there is the additional problem of solving the two-dimensional analogue of Poisson's equation, i.e. determining the wavefront surface given the wavefront gradients.

With MCAO the situation is much more complicated. Each deformable mirror affects the optical path at only one atmospheric layer, however each beacon integrates the optical path along the entire height of the atmosphere and probes (in the closed loop configuration) every deformable mirror. The multiple beacons at different field angles however do provide a means to resolve the height dependence in principle. The situation is similar to that of volumetric tomography where many beams at different angles are sent through the volume, detected on the other side, and then processed by a computer to produce a volumetric estimate.

MCAO has been traditionally handled in a "black box" manner. A certain number of measurements (Hartmann slopes) are given and a certain number of controls (deformable mirror actuators) are available. Through a prior calibration procedure, we know how the unit displacement of an actuator affects each output of the sensors. The solution (vector of actuator commands) is then the pseudo-inverse of the response matrix times the vector of wavefront sensor data. The matrix (in say the 30-meter telescope case) has dimensions in the tens of thousands, making it difficult to pseudo-invert accurately and costly to perform the matrix-vector multiplication in real time. The matrix is sparse however (a majority of the entries are zero or nearly zero) and implementations of MCAO reconstruction algorithms taking advantage of the sparseness have been successfully demonstrated in simulations[1].

An alternative approach, pursued in this paper, is to consider the MCAO problem from the standpoint of tomography. We follow the idea of Tokovinin and Viard[2] in initially formulating the problem in the Fourier domain. We then interpret the result in the spatial domain and show that the method naturally estimates the volumetric distribution of optical path changes through a process of tomographic back-projection of the measurements, followed by applying the negative of the optical path on a set of multi-conjugate deformable mirrors. The method is optimal (maximum Strehl for all field angles) in an ideal case where we assume infinite aperture, plane waves, and as many deformable mirrors as turbulent layers. It also produces (as we shall argue) an accurate solution for finite apertures, cone (laser guidestar) beams, and a finite number of deformable mirrors. We also derive an optimal spherical wave solution (the laser guide star case in the limit of infinite aperture).

The tomographic analysis lends itself particularly well to design studies since the design parameters for deformable mirrors, guidestars, etc. manifest themselves in the obvious stages of the algorithm. As an additional and fortuitous benefit, the technique generates an algorithm that can be feasibly implemented in real time. The resulting algorithm uses Fourier-domain filtering, small matrix inversions, and back projections, making it competitive with the sparse matrix methods.

2. TOMOGRAPHIC PHASE ESTIMATION WITH NATURAL GUIDE STARS

2.1 Least-squares solution

We consider a geometry (Figure 1) where multiple guidestar wavefronts having propagated through the atmosphere, are measured using separate wavefront sensors. Let $s_k(\mathbf{x})$ represent the output from the k'th wavefront sensor at aperture position $\mathbf{x}$ and $\phi(\mathbf{x},\boldsymbol{\theta}_k)$ the wavefront phase from the k'th guidestar, which is at field position $\boldsymbol{\theta}_k$. The spatial Fourier transform of the measurement is $\tilde{s}_k(\mathbf{f})$ where $\mathbf{f}$ represents spatial frequency. It is related to the wavefront phase through an operator $M(\mathbf{f})$, which is a gradient operator in the case of Hartmann wavefront sensors, and identity in the case of direct phase wavefront sensors,

$$\tilde{s}_k(\mathbf{f}) = M(\mathbf{f})\tilde{\phi}(\mathbf{f},\boldsymbol{\theta}_k) + \tilde{v}_k(\mathbf{f}) \qquad (1)$$

where $\tilde{v}_k(\mathbf{f})$ is the measurement noise.

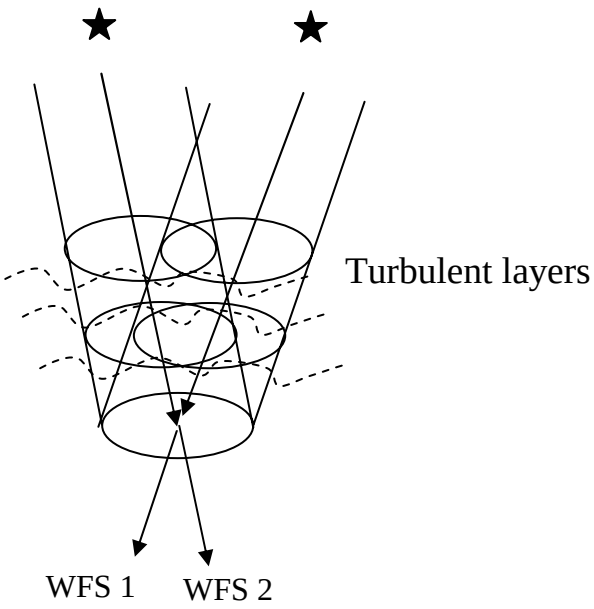

Figure 1. MCAO geometry

Following the approach of Tokovinin and Viard[2], we seek a minimum variance phase correction for starlight coming from a given science direction that is not necessarily coincident with any of the guidestars. The general solution is of the form

$$\tilde{\psi}(\mathbf{f},\boldsymbol{\theta}) = \sum_{k=1}^{N} \tilde{g}_k(\mathbf{f},\boldsymbol{\theta})\tilde{s}_k(\mathbf{f}) = \tilde{\mathbf{g}}^T\tilde{\mathbf{s}}\,, \tag{2}$$

where N is the number of guidestars and $\tilde{g}_k(\mathbf{f},\boldsymbol{\theta})$ is a vector of control gain quantities (one per guidestar per spatial frequency) yet to be determined. Note we have rewritten the sum as a vector dot-product and dropped the frequency argument.

In the case of traversal through weak turbulence, the effect on a wavefront is almost entirely in the phase and that phase is essentially the sum of the small optical path perturbations along the path,

$$\phi(\mathbf{x},\boldsymbol{\theta}) = \frac{2\pi}{\lambda}\int_0^\infty \delta n(\mathbf{x}-\boldsymbol{\theta}h)\mathrm{d}h \tag{3}$$

where h is the altitude above the telescope. The approximation ignores diffraction, i.e. it is a geometric ray approximation, but the weak turbulence at good astronomical sites justifies the approximation. The Fourier transform is

$$\tilde{\phi}(\mathbf{f},\boldsymbol{\theta}) = \frac{2\pi}{\lambda}\int_0^\infty \delta\tilde{n}(\mathbf{f})\exp(-2\pi i\mathbf{f}\cdot\boldsymbol{\theta}h)\mathrm{d}h\,. \tag{4}$$

We've adopt Tokovinin and Viard's sign convention for angle and sign convention in the Fourier transform (positive in the forward transform, negative in the inverse transform) in order to keep our notation as close as

possible to theirs. Equations (3) and (4) correspond to their equations (1) and (2) respectively. The power spectrum of δn in Kolmogorov turbulence is given by

$$W_{\delta n}(f,h) = 9.69\times10^{-3} C_n^2(h) |f|^{-11/3}. \tag{5}$$

The maximum Strehl of the corrected starlight image is achieved by minimizing the residual wavefront variance. The residual wavefront variance is minimized if each of the Fourier components in its power spectrum is minimized. The residual power spectrum, and the value of $\tilde{g}_k(\mathbf{f},\boldsymbol{\theta})$ that minimizes this power spectrum, are computed in Tokovinin and Viard. These are

$$W_\varepsilon(\mathbf{f}) = W_0(\mathbf{f}) c_0 \left[1 - 2\,\mathrm{Re}\left(\tilde{\mathbf{c}}^T \tilde{\mathbf{g}}\right) + \tilde{\mathbf{g}}^T \left(\tilde{\mathbf{A}} + \nu' \mathbf{I}\right) \tilde{\mathbf{g}}^*\right] \tag{6}$$

$$\begin{aligned}
&\tilde{\mathbf{g}}(\mathbf{f}) = \left[\left(\mathbf{A}(\mathbf{f}) + \upsilon'(\mathbf{f})\,\mathbf{I}\right)^{-1} \tilde{\mathbf{c}}(\mathbf{f})\right]^* \\
&\tilde{c}_k(\mathbf{f}) = M \int_0^\infty C_n^2(h) \exp\left[-2\pi i \mathbf{f}(\boldsymbol{\theta}_k - \boldsymbol{\theta}) h\right] dh \Big/ c_0 \\
&\tilde{a}_{kk'}(\mathbf{f}) = |M|^2 \int_0^\infty C_n^2(h) \exp\left[-2\pi i \mathbf{f}(\boldsymbol{\theta}_k - \boldsymbol{\theta}_{k'}) h\right] dh \Big/ c_0 \\
&c_0 = \int_0^\infty C_n^2(h)\, dh \\
&\upsilon'(\mathbf{f}) = W_\nu(\mathbf{f}) / \left(W_0(\mathbf{f}) c_0\right)
\end{aligned} \tag{7}$$

where $W_0(\mathbf{f}) = 9.69\times10^{-3} (2\pi/\lambda)^2 f^{-11/3}$. Several comments are in order.

The residual wavefront variance is the integral over all spatial frequencies of the residual power spectrum $W_\varepsilon(\mathbf{f})$. The residual power spectrum $W_\varepsilon(\mathbf{f})$ is a filtered version of the (uncorrected) height-integrated Kolmogorov phase power spectrum, $W_0(\mathbf{f}) c_0$. One would want this filter, which is a function of the correction gains and the noise-to-signal ratio, ν', to have a magnitude of much less than one over the range of spatial frequencies where Kolmogorov turbulence is significant. In the optimum gain case, the filter magnitude is in fact always less than or equal to one. To show this, we substitute the optimum gain (7) into (6), yielding

$$W_\varepsilon(\mathbf{f}) = W_0(\mathbf{f}) c_0 \left[1 - \mathbf{c}^T(\mathbf{f}) \left(\mathbf{A}(\mathbf{f}) + \upsilon'(\mathbf{f})\,\mathbf{I}\right)^{-1} \mathbf{c}^*\right]. \tag{8}$$

Since the matrix **A** is composed of an integral of vector outer products, the matrix **A**+ ν'**I** is positive-definite. Therefore the quantity in brackets, the turbulence suppression filter, is less than or equal to one at all frequencies.

From (7) we see that the matrix **A** is formed by considering all possible pairings of guidestars, and the vector **c** is formed by considering pairings of each guidestar with the science target. **A+I**ν' is a square matrix with dimension equal to the number of guidestars. It must be inverted at each spatial frequency.

2.2 Wavefront slope sensor model

The role of the measurement operator M in the optimum gain case is interesting. For example, in the zero noise case the control gain **g** is proportional to M^{-1}, which means that the first step in the wavefront correction process is simply to invert the measurement operation to produce a direct measure of phase. Note also that in this case M cancels out of the expression for residual variance. In the finite noise case, the effect on gain and residual variance is the same as if the phase were directly measured, but had a noise spectrum shaped by the inverse of the measurement operator. Given the trivial role of the scalar, invertible measurement operator we can assume without loss of generalilty that M=1.

However, the Hartmann sensor presents a special situation. In the Hartmann sensor case, $M(\mathbf{f})$ is a two vector, $2\pi(if_x, if_y)$, corresponding to gradients the two directions. Thus the "$|M|^2$" factor in $a_{kk'}$ is really a matrix

$$MM^{*T} = 4\pi^2 \begin{bmatrix} f_x^2 & f_x f_y \\ f_x f_y & f_y^2 \end{bmatrix}. \tag{9}$$

The matrix is singular and therefore not invertible. Tokovinin and Viard deal with this by ignoring the cross terms. With further investigation, we can take a more exact approach. From the two slope measurements s_x and s_y we form the invertible linear transformation:

$$\begin{pmatrix} \tilde{s}_0 \\ \tilde{s}_1 \end{pmatrix} = \begin{pmatrix} if_x & if_y \\ -if_y & if_x \end{pmatrix} \begin{pmatrix} \tilde{s}_x \\ \tilde{s}_y \end{pmatrix} = -2\pi \begin{pmatrix} f_x^2 + f_y^2 \\ 0 \end{pmatrix} \tilde{\phi} + \begin{pmatrix} if_x \tilde{v}_x + if_y \tilde{v}_y \\ -if_y \tilde{v}_x + if_x \tilde{v}_y \end{pmatrix}. \tag{10}$$

It is easy to see that only one linear combination, corresponding to the divergence of slopes, depends on the phase. The other linear combination, corresponding to the curl of slopes, has no dependence on phase. Therefore there is only one useful measurement actually produced by the Hartmann sensor, the Laplacian of the phase, with a noise term equal to the divergence of an uncorrelated noise field. Replacing the two slope measurements s_x, s_y, with the single measurement s_0, divergence of slopes, the measurement operator becomes a scalar, $M = -2\pi(f_x^2+f_y^2)$. Now in the zero noise case, the inversion of the measurement operator is possible at all but one spatial frequency, **f** = 0. This particular spatial frequency corresponds to the pure piston mode, to which the Hartmann sensor is blind.

Therefore, even in the Hartmann sensor case, the measurement can be represented as a scalar operation, which is the Laplacian operator. Since this is an invertible linear operator (except at **f** = 0), we can invoke our earlier argument and assume without loss of generality that the wavefront sensors actually measure phase directly, with a measurement noise that has a power spectrum of $\sigma^2/2\pi f^2$ where σ^2 is the slope measurement error and $f^2 = f_x^2+f_y^2$.

3. INTERPRETING THE SINGLE GUIDESTAR CASE AS BACK PROJECTION

We will demonstrate that Tokovinin and Viard's MCAO reconstruction process, (7) is a sequence of tomographic back-projections of filtered beacon measurements, followed by a forward projection in the science direction. To motivate the discussion, and provide a simple example, we consider the case of a single natural guidestar in one direction and a single science object in another. In this case, $\mathbf{A} = a_{11} = 1$, and, in the no-noise case, $\mathbf{g} = \mathbf{c}^*$ or

$$\tilde{\psi}(\mathbf{f},\boldsymbol{\theta}) = \int_0^\infty C_n^2(h)\tilde{s}_1(\mathbf{f})\exp\left[-2\pi i\mathbf{f}\cdot(\boldsymbol{\theta}-\boldsymbol{\theta}_1)h\right]dh \Big/ c_0 . \tag{11}$$

The inverse Fourier transform is

$$\psi(\mathbf{x},\boldsymbol{\theta}) = \int C_n^2(h) s_1(\mathbf{x} - (\boldsymbol{\theta} - \boldsymbol{\theta}_1)h) dh \quad / c_0 \,. \tag{12}$$

The shifts in the two directions imply that the solution can be divided into two parts. We define a volumetric estimate of optical path perturbations, given measurement s_1, as

$$\delta n_{est}(\mathbf{x}, h) = \frac{\lambda}{2\pi c_0} C_n^2(h) s_1(\mathbf{x} + \boldsymbol{\theta}_1 h) \,. \tag{13}$$

Then the estimated phase in the science direction becomes

$$\psi(\mathbf{x},\boldsymbol{\theta}) = \frac{2\pi}{\lambda} \int \delta n_{est}(\mathbf{x} - \boldsymbol{\theta} h, h) dh \tag{14}$$

which satisfies (12). The volumetric estimate (13) is simply a back-propagation, along the path of the guidestar light, of the phase measured by wavefront sensor 1. Note that this back-propagation is not uniformly smeared but is weighted with altitude according to the normalized C_n^2 profile, i.e. by the relative expected turbulence strength. Also note that the back-propagation is along the path to the guidestar and does not depend on the science direction. The wavefront correction in the science direction is given by (14), which is simply the forward propagation, along the science ray paths, through the turbulence volume that was estimated by the back projection step.

When there is noise, the volumetric estimate is filtered by the factor 1/(1+ν'), which is a frequency-dependent quantity depending on the noise-to-signal ratio.

4. THE MULTIPLE GUIDESTAR CASE: MATRIX-FILTERED BACK PROJECTION

From (7)

$$\begin{aligned} \tilde{\psi}(\mathbf{f},\boldsymbol{\theta}) &= \tilde{\mathbf{c}}^{*T}(\mathbf{f}) \left[\mathbf{A}^*(\mathbf{f}) + \mathbf{I}\nu'^*(\mathbf{f})\right]^{-1} \tilde{\mathbf{s}}(\mathbf{f}) \\ &= \int_0^\infty \exp(-2\pi i \mathbf{f}\cdot\boldsymbol{\theta} h) \sum_{k=1}^N \sum_{k'=1}^N \tilde{\alpha}_{kk'}(\mathbf{f}) C_n^2(h) \exp(2\pi i \mathbf{f}\cdot\boldsymbol{\theta}_{k'} h) \tilde{s}_k(\mathbf{f}) dh \Big/ c_0 \end{aligned} \tag{15}$$

where $\alpha_{kk'}(\mathbf{f})$ are the elements of $(\mathbf{A}+\mathbf{I}\nu)^{-1}$. We define a filtered sensor vector $\mathbf{s}'$

$$\tilde{\mathbf{s}}'(\mathbf{f}) = \left[\mathbf{A}^*(\mathbf{f}) + \mathbf{I}\nu'^*(\mathbf{f})\right]^{-1} \tilde{\mathbf{s}}(\mathbf{f}) \,. \tag{16}$$

Then, taking the inverse Fourier transform of (15), we have

$$\psi(\mathbf{x},\boldsymbol{\theta}) = \int_0^\infty C_n^2(h) \sum_{k=1}^N s'_k(\mathbf{x} - (\boldsymbol{\theta} - \boldsymbol{\theta}_k)h) \mathrm{d}h \Big/ c_0 \,. \tag{17}$$

Now define the volumetric estimate of turbulence as

$$\delta n(\mathbf{x}, h) = \frac{\lambda}{2\pi c_0} \sum_{k=1}^N s'_k(\mathbf{x} + \boldsymbol{\theta}_k h) C_n^2(h) \tag{18}$$

which is the sum of back projections of the filtered wavefront measurements. The filter, being a matrix, mixes combinations of all the original guidestar measurements s_k to produce a new measurement vector s'_k. This matrix filter depends only on the directions of the guide stars and not at all on the direction of the science object. Each element of this new measurement vector is then projected back along the direction of the correspondingly indexed guide star, weighted with altitude by the normalized C_n^2 profile.

The wavefront estimate in the science direction (17) is then written as

$$\psi(\mathbf{x},\boldsymbol{\theta}) = \frac{2\pi}{\lambda}\int \delta n(\mathbf{x} - \boldsymbol{\theta}h, h)dh \tag{19}$$

i.e. it is the forward propagation along the science direction through the estimated turbulence volume.

The filtering of wavefront sensor measurements plays an important role. It assures that the solution is consistent with the data, which would not be the case if multiple wavefront measurements were simply back propagated through the volume and added together. For example imagine two guidestars each back propagated in turn in a noise-free case. After the back propagation of one guidestar, a forward propagation from that guidestar direction will reproduce the measurement. If however, a second guidestar's measurement is then back propagated and added to the volume estimate, then a forward propagation from either guidestar will not reproduce its measurement. One could iterate on this process (repeating the cycle of back projections and updating with the residuals until consistency is reached), but experience has shown that convergence rates are very slow.

Now consider using the filter. If the "science" direction is along the direction to one of the guidestars, $\boldsymbol{\theta} = \boldsymbol{\theta}_k$ then, from equation (7) the **c** vector is equal to one of the rows of **A**. Multiplying $\mathbf{c}^T$ by $\mathbf{A}^{-1}$ (in the noise-free case) will produce a vector with a 1 at that guidestar's index and a zero at all others. Thus the forward propagation along any guidestar direction reproduces the measurement from that guidestar. The filtered back-projection avoids the artifacts, inconsistencies, and slow convergence that an unfiltered back projection algorithm would cause.

5. FINITE APERTURE BACK PROJECTIONS

5.1 Procedure: mimic the infinite aperture method

In the finite aperture case, the measured wavefronts, s_k, are provided only over the aperture of diameter D.

$$s_k^{FA}(\mathbf{x}) = s_k(\mathbf{x})p(\mathbf{x};D) \tag{20}$$

where p(x;D) equals one inside the aperture and zero outside. The Fourier transform of infinite-aperture wavefront multiplied by the pupil function is simply the Fourier transform of the infinite-aperture wavefront convolved with the Fourier transform of the pupil function:

$$\tilde{s}_k^{FA}(\mathbf{f}) = \tilde{s}_k(\mathbf{f}) \otimes \tilde{p}(\mathbf{f};D). \tag{21}$$

If we execute the back projection process of equation (18), but this time with the finite aperture beams, the result will be a volumetric estimate of index variations, but only over the space defined by collimated beams from each guidestar. Since the matrix **A**(**f**) does not depend on the aperture function, the transform of the filtered finite-aperture wavefront also is a convolution of the infinite-aperture filtered wavefront with the transform of the pupil function. The net effect is error in the solution at frequency domain scales smaller than 1/D.

5.2 Simulation results

While this approach is not proven to be optimal, it is reasonably accurate. We ran a simulation under typical conditions for a 30 meter telescope at a reasonably good site. The conditions were r_0 = 20 cm, and a Cerro Pachon 6-layer C_n^2 profile[1]. Uncompensated wavefront error is 5.2 microns rms under these conditions. We used 5 guidestars in a "dice" constellation (4 guidestars on a circle of radius of 50 arcsec and one in the middle). Science directions were evaluated at 10, 25, and 45 arcseconds from the center along an azimuth line at 45 degrees from a line to one of the guidestars. The graph in Figure 2 shows a comparison of results from simulations of the infinite aperture and finite aperture cases.

An "extension" method that improves the solution accuracy of the finite aperture case is discussed in Section 7 below.

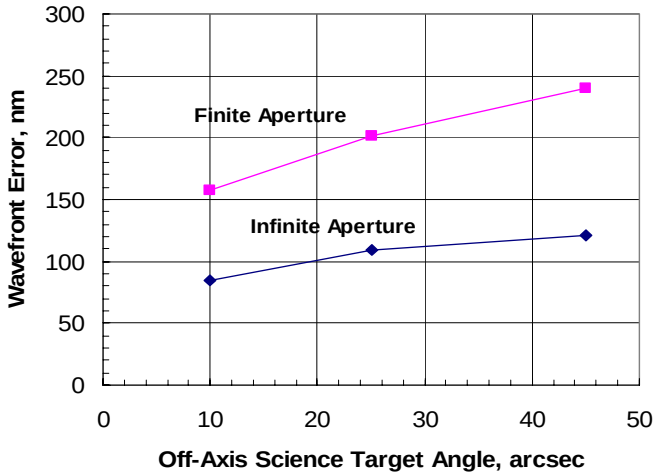

Figure 2. Comparison of residual phase error after MCAO correction for the infinite aperture and finite aperture plane wave cases. Uncorrected phase error is 5.2 microns rms.

6. LASER GUIDE STARS: SPHERICAL WAVE BACK PROPAGATION

Up to now, we have assumed that light from the guide stars comes from infinity, that is, is in the form of plane waves. Laser guide stars at finite altitude produce spherical waves. In this section we derive the optimum tomographic solution for spherical waves. We show that this solution is similar to the back projection process of equation (18), but modified by appropriate scaling of estimates in space (or frequency) with height, *h*. With a finite aperture, the laser beacon beams sweep out cones, not columns and so, analogous to the discussion in Section 6, we argue that an accurate reconstruction is obtained by back propagating along the cone beams in a manner that emulates the optimal spherical wave solution.

The measurement from laser guide star *k* is

$$s_k(\mathbf{x}) = \phi(\mathbf{x}, \boldsymbol{\theta}_k) + \nu_k = \frac{2\pi}{\lambda}\int_0^z \delta n\left(\mathbf{x}\frac{z-h}{z} - \boldsymbol{\theta}_k h, h\right)\mathrm{d}h + \nu_k \qquad (22)$$

where *z* is the altitude of the guide star. (We have once again assumed $M \equiv 1$ here, which is without loss of generality as explained in Section 2.2). Taking the Fourier transform,

$$\tilde{s}_k(\mathbf{f}) = \frac{2\pi}{\lambda}\int_0^z \left(\frac{z}{z-h}\right)^2 \delta\tilde{n}\left(\mathbf{f}\frac{z}{z-h}, h\right)\exp\left(-2\pi i\mathbf{f}\cdot\boldsymbol{\theta}_k\frac{z}{z-h}h\right)\mathrm{d}h + \tilde{v}_k. \tag{23}$$

The most general solution possibility would be that any spatial frequency in the data might contribute to a given spatial frequency in the optimal solution:

$$\delta\tilde{n}_{est}(\mathbf{f}, h) = \frac{\lambda}{2\pi}\int\sum_k \tilde{G}_k(\mathbf{f}, \mathbf{f}', h)\tilde{s}_k(\mathbf{f}')\mathrm{d}f'. \tag{24}$$

Along the science direction, $\boldsymbol{\theta}$, the wavefront error is

$$\begin{aligned}\tilde{\varepsilon}(\mathbf{f}, \boldsymbol{\theta}) &= \tilde{\phi}(\mathbf{f}, \boldsymbol{\theta}) - \tilde{\psi}(\mathbf{f}, \boldsymbol{\theta}) \\ &= \frac{2\pi}{\lambda}\int_0^z \left[\delta\tilde{n}(\mathbf{f}, h) - \int\sum_k \tilde{G}_k(\mathbf{f}, \mathbf{f}', h)\tilde{s}_k(\mathbf{f}')\mathrm{d}\mathbf{f}'\right]\exp(-2\pi i\mathbf{f}\cdot\boldsymbol{\theta}h)\mathrm{d}h\end{aligned} \tag{25}$$

The objective is to minimize the mean square wavefront error variance, $\left\langle\tilde{\varepsilon}^2\right\rangle$. In Appendix A we show that since $\left\langle\delta\tilde{n}(\mathbf{f}, h)\delta\tilde{n}(\mathbf{f}', h')\right\rangle = W_{\delta n}(\mathbf{f}, h)\delta(\mathbf{f}-\mathbf{f}')\delta(h-h')$ where $W_{\delta n}(\mathbf{f}, h) = 9.69\times10^{-3}C_n^2(h)f^{-11/3}$ solutions will be restricted to linear filters of the form

$$\delta\tilde{n}_{est}(\mathbf{f}, h) = \frac{\lambda}{2\pi}\sum_k \tilde{g}_k(\mathbf{f}, h)\,\tilde{s}_k\left(\mathbf{f}\frac{z-h}{z}\right). \tag{26}$$

Taking the inverse Fourier transform of (26) the expression for the volumetric index estimate is

$$\delta n_{est}(\mathbf{x}, h) = \frac{\lambda}{2\pi}\left(\frac{z}{z-h}\right)^2\sum_k g_k^s(\mathbf{x}, h)\otimes s_k\left(\mathbf{x}\frac{z}{z-h} + \boldsymbol{\theta}_k h\right) \tag{27}$$

where $\otimes$ denotes the convolution operator. Equation (27) highlights the fact that the wavefront measurement data are being compressed laterally with increasing altitude, which is exactly what one would expect when back-propagating a spherical wave.

From Appendix A, the filter gains $\tilde{\mathbf{g}}^s(\mathbf{f}, h)$ that minimize the mean square error are given by:

$$\tilde{\mathbf{g}}^s(\mathbf{f}, h) = \left\{\left[\mathbf{A}^s\left(\mathbf{f}\frac{z-h}{z}\right) + \mathbf{V}'\left(\mathbf{f}\frac{z-h}{z}\right)\right]^{-1}\mathbf{c}^s(\mathbf{f}, h)\right\}^* \tag{28a}$$

where

$$c_k^s(\mathbf{f},h) = \left(z/(z-h)\right)^{-11/3} C_n^2(h)\exp\left(-2\pi i\mathbf{f}\cdot\boldsymbol{\theta}_k h\right)\ /c_0$$
$$a_{kk'}^s(\mathbf{f}) = \int_0^z \left(z/(z-h')\right)^{-5/3} C_n^2(h')\exp\left(2\pi i\mathbf{f}\cdot(\boldsymbol{\theta}_{k'}-\boldsymbol{\theta}_k)h'\right)\mathrm{d}h'\ /c_0 \qquad (28b)$$
$$v'_{kk'}(\mathbf{f}) = v_k^2(\mathbf{f})\delta_{kk'}/\left(9.69\times10^{-3} f^{-11/3} c_0\right)$$

Combining (27) and (28)

$$\delta n_{est}(\mathbf{x},h) = \frac{\lambda}{2\pi}\left(\frac{C_n^2(h)}{c_0}\right)\sum_{k=1}^{N} s'_k\left(\mathbf{x}\frac{z}{z-h} + h\boldsymbol{\theta}_k\right). \qquad (29)$$

where s'_k is the result of filtering s_k with $\left(\mathbf{A}^s(\mathbf{f}) + v'(\mathbf{f})\mathbf{I}\right)^{-1}$ The algorithm can be described as follows.

1. Take the Fourier transform of each guidestar's wavefront measurement.

2. Filter according to $\left[\mathbf{A}^s(\mathbf{f}) + v'(\mathbf{f})\mathbf{I}\right]^{-1}$. Note that the filter for spherical waves is different from that of plane waves (7) because of the altitude dependent expansion of frequencies in the integrations.

3. Back propagate the filtered data, weighting by $C_n^2(h)$ as before, along paths back to the guidestars, and compressing the data (in space) linearly with altitude by the factor $(z-h)/z$. Equivalently, the back-propagation can be done in the spatial frequency domain, increasing the spatial frequencies with altitude by the factor $z/(z-h)$.

7. LASER GUIDE STARS AND FINITE APERTURES

7.1 Back projection

As in Section 5, imposing the finite aperture poses no immediate difficulty in employing the filtered back projection described by (28) along the cones reaching back to the guide stars. Error is concentrated near the boundaries and outside of the beam volumes.

7.2 Extension

Back projection of finite apertures is not as accurate as in the infinite aperture case. But since phase aberrations outside the aperture are correlated to phase aberrations inside the aperture, via Kolmogorov spatial statistics, an "extension" of the in-pupil phase measurements to points outside the pupil can be accomplished by a minimum-variance estimation process. Consider the phase $\phi_A(\mathbf{x}) = \phi(\mathbf{x})P(\mathbf{x};D)$ which is inside the aperture and the phase $\phi_{\bar{A}}(\mathbf{x}) = \phi(\mathbf{x})[1-P(\mathbf{x};D)]$ which is outside. One can estimate the (unmeasured) phase outside via a least-squares estimate

$$\phi_{\bar{A}}(\mathbf{x}) = \int_A L(\mathbf{x},\mathbf{x}')\phi_A(\mathbf{x}')\mathrm{d}\mathbf{x}' \qquad (30)$$

where $L(\mathbf{x},\mathbf{x}')$ is the solution to the integral equation

$$\left\langle \phi_{\bar{A}}(\mathbf{x})\phi_A(\mathbf{x}')\right\rangle = \int L(\mathbf{x},\mathbf{x}'')\left\langle \phi_A(\mathbf{x}')\phi_A(\mathbf{x}'')\right\rangle \mathrm{d}\mathbf{x}''. \qquad (31)$$

Expressions for the cross-covariance of piston-removed phase under the Kolmogorov power spectrum are given in references 3 and 4. We have not yet developed a satisfactory method for solving these extension equations in the Fourier domain; this work is still in progress. However, we did solve them with a discrete approximation in the spatial domain and used the results in back propagation tomography in order to determine how much the numerical accuracy of the solution can be improved.

7.3 Simulation results

Simulation parameters are the same as in section 5, except that the guidestars are located at 90 km altitude instead of infinity. Figure 3 summarizes results. Extension recovers some of the error introduced by aperture truncation, but does not lower the error to the level of the infinite aperture case.

We show in Figure 4 a comparison of the finite aperture result (with extension) to that of Brent Ellerbroek's LAOS/TAOS code results of the same simulation case. LAOS/TAOS is a sparse-matrix minimum-variance MCAO solver/simulator based on spatial domain covariance matrix inversion[1]. Results agree quite closely, indicating that the the back-projection algorithm is achieving minimum-variance residuals, but only if we employ extension.

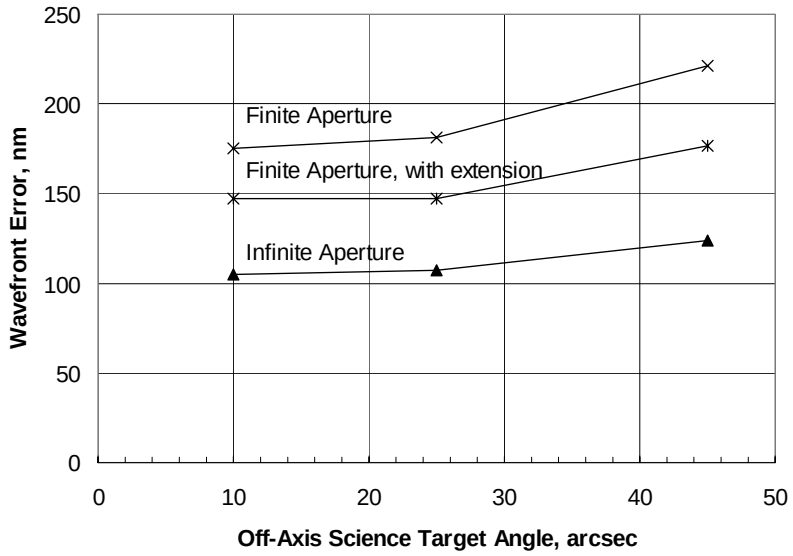

Figure 3. Spherical wave simulation results. With extension, the finite aperture case can achieve lower residual wavefront error, but not as low as the infinite aperture case.

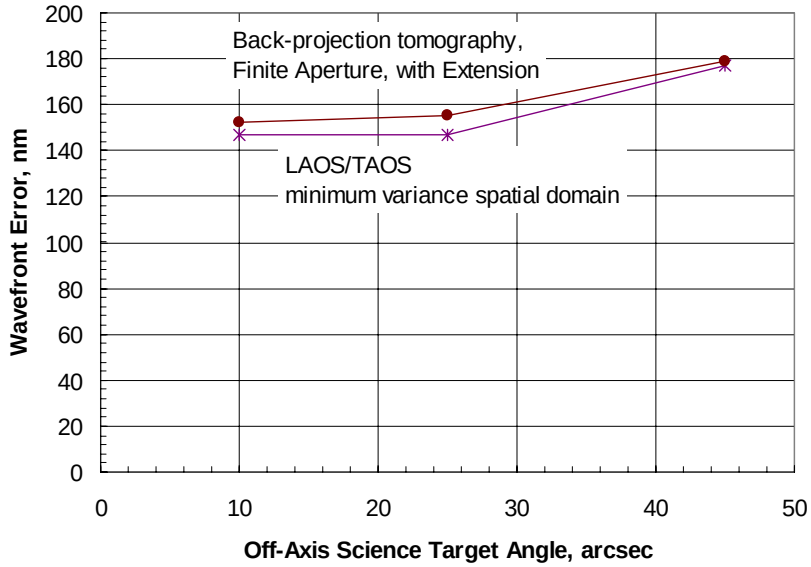

Figure 4. Comparison of back-projection tomography method with a minimum-variance spatial domain method, LAOS/TAOS[1]

7.4 Cone effect in MCAO

Cone effect in a traditional ground-layer conjugate AO system is the result of to two error processes:

1. The lateral stretching of phase aberrations from higher altitudes by the laser guidestar probe is not accounted for in the correction. Thus high spatial frequency aberrations at high altitudes become low spatial frequency corrections. The majority of traditional cone effect is due to this error.

2. The failure to probe high altitude turbulence which is outside the metapupil of the finite-apertured cone beam but inside the metapupil of the science field. On axis with the guide star, this effect is minor compared to the stretching error.

Cone effect for MCAO can be expressed in terms of the difference between theoretical residual variance for spherical waves, as given by equation (A14), and the same for plane waves (equation 8).

8. PROJECTION ONTO DEFORMABLE MIRRORS AT CONJUGATE PLANES

8.1 Plane wave case

From Tokovinin, Le Louarn, and Sarazin[5], the deformable mirror actuator commands can be derived from volumetric index variations according to

$$\tilde{d}_m(f) = \int \tilde{g}_m^{DM}(f,h)\delta\tilde{n}(f,h)dh \qquad (32)$$

where $d_m(x)$ is the phase to be commanded on deformable mirror *m*. The "compaction" kernal $\tilde{g}_m^{DM}(f,h)$ that gives the minimum amount of anisoplanatism is found[2] to be

$$\begin{aligned}\tilde{\mathbf{g}}^{DM}(f,h) &= \mathbf{A}^{DM\,-1}(f)\tilde{\mathbf{b}}^{DM}(f,h)\\ \tilde{b}^{DM}_{m'} &= J_0\left[2\pi f\Theta(H_m - h)\right]\\ \tilde{a}^{DM}_{mm'} &= J_0\left[2\pi f\Theta(H_m - H_{m'})\right]\end{aligned} \quad . \tag{33}$$

where Θ is the half-angle of the field-of-view and H_m are the conjugate heights of the DMs. One can combine the two steps of back propagation and compaction onto DMs by substituting (18) and (33) into (32). This yields a formulation of mirror controls in terms of a reconstruction matrix (in the frequency domain) times filtered wavefront measurements:

$$\begin{aligned}\tilde{d}_m(f) &= \int \tilde{g}^{DM}_m(f,h)\delta\tilde{n}(f,h)dh\\ &= \sum_{k,m'}\left\{\left[\mathbf{A}^{DM}\right]^{-1}_{mm'}(f)\int C_n^2(h)b^{DM}_{m'}(f,h)e^{2\pi ifh\theta_k}dh\right\}\tilde{s}'_k(f)\\ \tilde{d}_m(f) &= \sum_k P^{DM}_{mk}(f)\tilde{s}'_k(f)\end{aligned} \tag{34}$$

As a simple approximation, and to serve as insight into the process, we consider the case where the atmospheric layers correspond exactly to altitudes where the DMs are placed, that is, $C_n^2(h) = \sum_m c^2_{nm}\delta(h - H_m)$ and $\sum_m c^2_{nm} = c_0$.

In that case it is easy to show using (31) that

$$\tilde{g}_m(f, H_{m'}) = \delta_{mm'} \tag{35}$$

and the process of finding DM commands is simply one of back projecting the filtered wavefront measurements to the DM conjugate altitudes, appropriately shifted at each height:

$$\tilde{d}_m(f) = \sum_k c^2_{nm}e^{2\pi ifH_m\theta_k}\tilde{s}'_k(f). \tag{36}$$

8.2 Spherical wave case

Equations (30) and (31) still apply, but substitute (26) instead of (18).

9. ADDITIONAL ISSUES

9.1 Undefined piston with slope sensors

Applying the Fourier domain based procedure to finite apertures presents two difficulties. The first is the possibility of aperture-size piston terms which are invisible to the Hartmann slope sensors. The failure to back propagate the correct piston terms may result in phase stitching errors in the higher altitude layers. Simulations seem to show that if the guidestars are placed to sufficiently overlap higher altitude meta-pupils, then the piston induced errors are negligible.

9.2 Phase from slopes on a finite aperture

There have been many methods utilized to calculate the phase given the slope measurements provided by a Hartmann sensor[6]. In Section 2.2 we described how the process is basically inversion of Poisson's equation in the Fourier domain. However, there is a problem with working in the Fourier domain in the case a finite aperture. Significant errors in the reconstructed phase result if one assumes slopes are zero outside the aperture. The algorithm of Poyneer, Gavel, and Brase[7] solves this problem by employing boundary conditions that assure that the wavefront gradient field is curl-free everywhere including across and outside the aperture boundary. The phase from slopes calculation is then exact inside the aperture.

9.3 Undefined tip/tilt with laser guidestars

Laser guide stars are not a good source of tip/tilt information since the laser beam wanders on the up-path through the atmosphere. The traditional solution in single-conjugate LGS AO systems is to use a natural star for tip/tilt information. We have not dealt with that issue in this paper, having assumed all wavefront information is available to the wavefront sensors both in our theoretical development and in the simulations. A refinement of the development here will be to incorporate noisy tip/tilt measurements from natural stars (and ignoring the tip/tilt of the laser stars) into the overall tomographic process. This is the subject of future work.

9.4 Closed-loop control considerations

In this paper we have not made any considerations of how the tomography algorithm should be implemented in closed loop. A Kalman filter and a wind or turbulence progression model would have to be employed for optimal repeated updates of the volumetric estimate[4, 8]. Stability of any closed loop implementation would have to be proven. One alternative, proposed by Ellerbroek and Vogel, is a method called pseudo-open-loop feedback control[9], where essentially measurements of residuals are added to prior estimates of phase to generate a pseudo open loop measurement, which is then run through the tomography procedure. This approach has been shown to be stable in simulations.

10. CONCLUSIONS

We have presented the basis for using back-projection tomography to solve the multi-conjugate adaptive optics problem. The method works for both plane wave (natural guide star) and spherical wave (laser guide star) beacons. Through a minimum-variance extension procedure, some of the information lost in the truncation at a finite aperture is recovered and the process has been shown in simulation to be as accurate as spatial domain minimum-variance matrix pseudo-inverse methods.

A. APPENDIX – DERIVATION OF EQUATION 26

For the following analysis it is important to understand the properties of the 2-dimensional Dirac delta-function. The delta-function is defined in terms of its 'sifting' behavior inside an integral:

$$\int_{-\infty}^{\infty} f(\mathbf{x})\delta(\mathbf{x}-\mathbf{x}_0)\mathrm{d}\mathbf{x} = f(\mathbf{x}_0), \tag{A1}$$

from which we can derive two useful properties:

$$\delta(\alpha\mathbf{x}) = \frac{1}{\alpha^2}\delta(\mathbf{x}) \tag{A2a}$$

$$\tilde{\delta}(\mathbf{f}) = \int_{-\infty}^{\infty} \delta(\mathbf{x})\exp(-2\pi i\mathbf{f}\cdot\mathbf{x})\mathrm{d}\mathbf{x} = 1 \tag{A2b}$$

Taking the inverse Fourier transform of (A2b) it follows that

$$\int_{-\infty}^{\infty} \exp(2\pi i \mathbf{f}\cdot\mathbf{x})\mathrm{d}\mathbf{f} = \delta(\mathbf{x}). \tag{A2c}$$

We will also use properties of power spectral density, which is formally defined as the Fourier transform of the autocorrelation function. For Kolmogorov turbulence, which has infinite variance, the definition of power spectral density has been extended usefully by Noll[10], to equal minus one-half the Fourier transform of the structure function. The Fourier components of Kolmogorov random screens are delta-correlated

$$\left\langle \delta\tilde{n}(\mathbf{f},h)\delta\tilde{n}^*(\mathbf{f}',h')\right\rangle = W_{\delta n}(f,h)\delta(\mathbf{f}-\mathbf{f}')\delta(h-h') \tag{A3}$$

where $W_{\delta n}(f,h)$ is the power spectral density of $\delta n(x,h)$, defined in (5). The delta-correlation with height *h* is the usual assumption for turbulent layers in the atmosphere. The delta-correlation in spatial frequency is a consequence of the definition of power spectrum and property (A2c).

Starting with the expression for error in (25) we take the expected square error

$$\begin{aligned}\left\langle \tilde{\varepsilon}^2(\mathbf{f},\boldsymbol{\theta})\right\rangle = \left(\frac{2\pi}{\lambda}\right)^2 \int_0^z\int_0^z \Big[&\left\langle \delta\tilde{n}(\mathbf{f},h)^2\right\rangle \delta(h-h') - 2\,\mathrm{Re}\int \sum_k \tilde{G}_k^*(\mathbf{f},\mathbf{f}',h')\left\langle \delta\tilde{n}(\mathbf{f},h)\tilde{s}_k^*(\mathbf{f}')\right\rangle \mathrm{d}\mathbf{f}' \\ &+ \iint \sum_k\sum_{k'} \tilde{G}_k(\mathbf{f},\mathbf{f}',h')\tilde{G}_{k'}^*(\mathbf{f},\mathbf{f}'',h)\left\langle \tilde{s}_k(\mathbf{f}')\tilde{s}_{k'}^*(\mathbf{f}'')\right\rangle \mathrm{d}\mathbf{f}'\mathrm{d}\mathbf{f}''\Big] \exp(2\pi i\mathbf{f}\cdot\boldsymbol{\theta}(h'-h))\,\mathrm{d}h\,\mathrm{d}h'\end{aligned} \tag{A4}$$

Taking the partial derivative with respect to gains $\tilde{G}_k^*(\mathbf{f},\mathbf{f}',h')$ and setting equal to zero results in the following expression for the gain that produces the minimum mean square error:

$$\left\langle \delta\tilde{n}(\mathbf{f},h)\tilde{s}_k^*(\mathbf{f}')\right\rangle = \int \sum_{k'} \tilde{G}_{k'}(\mathbf{f},\mathbf{f}'',h)\left\langle \tilde{s}_k^*(\mathbf{f}')\tilde{s}_{k'}(\mathbf{f}'')\right\rangle \mathrm{d}\mathbf{f}'' \tag{A5}$$

We now can introduce expressions for the cross-correlation of measured data to index, and measured data to measured data. Correlation of measured data to index is

$$\begin{aligned}\left\langle \delta\tilde{n}(\mathbf{f},h)\tilde{s}_k^*(\mathbf{f}')\right\rangle &= \int_0^z \left(\frac{z}{z-h'}\right)^2 \left\langle \delta\tilde{n}(\mathbf{f},h)\delta\tilde{n}\left(\mathbf{f}'\frac{z}{z-h'},h'\right)\right\rangle \exp\left(2\pi i\mathbf{f}'\cdot\boldsymbol{\theta}_k\frac{z}{z-h'}h'\right)\mathrm{d}h' \\ &= \left(\frac{z}{z-h}\right)^2 W_{\delta n}(f,h)\delta\left(\mathbf{f}-\mathbf{f}'\frac{z}{z-h}\right)\exp\left(2\pi i\mathbf{f}'\cdot\boldsymbol{\theta}_k\frac{z}{z-h}h\right) \\ &= W_{\delta n}(f,h)\exp(2\pi i\mathbf{f}\cdot\boldsymbol{\theta}_k h)\,\delta\left(\mathbf{f}\frac{z-h}{z}-\mathbf{f}'\right)\end{aligned} \tag{A6}$$

where in the last step we used the scaling law of delta-functions, (A2a). Correlation of measured data to measured data (minus the noise covariance contribution) is:

$$
\begin{aligned}
&\left\langle \tilde{s}_k^*(\mathbf{f}')\tilde{s}_{k'}(\mathbf{f}'')\right\rangle - v_k^2(\mathbf{f}')\delta(\mathbf{f}'-\mathbf{f}'')\delta_{kk''} = \\
&= \int_0^z \left(\frac{z}{z-h}\right)^4 \left\langle \delta\tilde{n}\left(\mathbf{f}'\frac{z}{z-h},h\right)\delta\tilde{n}\left(\mathbf{f}''\frac{z}{z-h},h\right)\right\rangle \exp\left(2\pi i(\mathbf{f}'\cdot\boldsymbol{\theta}_k - \mathbf{f}''\cdot\boldsymbol{\theta}_{k'})\frac{z}{z-h}h\right)\mathrm{d}h \\
&= \int_0^z \left(\frac{z}{z-h}\right)^4 W_{\delta n}\left(f'\frac{z}{z-h},h\right)\delta\left((\mathbf{f}'-\mathbf{f}'')\frac{z}{z-h}\right)\exp(2\pi i\mathbf{f}'\cdot(\boldsymbol{\theta}_k-\boldsymbol{\theta}_{k'})h)\mathrm{d}h \\
&= \int_0^z \left(\frac{z}{z-h}\right)^{-5/3} W_{\delta n}(f',h)\exp(2\pi i\mathbf{f}'\cdot(\boldsymbol{\theta}_k-\boldsymbol{\theta}_{k'})h)\mathrm{d}h\ \delta(\mathbf{f}'-\mathbf{f}'')
\end{aligned}
\tag{A7}
$$

where in the last step we used the scaling law of delta-functions and the fact that $W_{\delta n}(f,h)$ scales in magnitude with spatial frequency according to $f^{-11/3}$. Substituting into (A5):

$$
\begin{aligned}
&W_{\delta n}(f,h)\exp(2\pi i\mathbf{f}\cdot\boldsymbol{\theta}_k h)\,\delta\left(\mathbf{f}\frac{z-h}{z}-\mathbf{f}'\right) \\
&= \sum_{k'}\tilde{G}_{k'}(\mathbf{f},\mathbf{f}',h)\left[\int_0^z\left(\frac{z}{z-h'}\right)^{-5/3} W_{\delta n}(f',h')\exp(2\pi i\mathbf{f}'\cdot(\boldsymbol{\theta}_k-\boldsymbol{\theta}_{k'})h')\mathrm{d}h' + v_k^2(\mathbf{f}')\right]
\end{aligned}
\tag{A8}
$$

Therefore a minimum-mean-square error solution must be of the form

$$
\tilde{G}_k(\mathbf{f},\mathbf{f}',h) = \tilde{g}_k(\mathbf{f},h)\,\delta\left(\mathbf{f}'-\mathbf{f}\frac{z-h}{z}\right) \tag{A9}
$$

which converts (24) into the desired form (26)

$$
\delta\tilde{n}_{est}(\mathbf{f},h) = \frac{\lambda}{2\pi}\int\sum_k \tilde{G}_k(\mathbf{f},\mathbf{f}',h)\tilde{s}_k(\mathbf{f}')d\mathbf{f}' = \frac{\lambda}{2\pi}\sum_k \tilde{g}_k(\mathbf{f},h)\,\tilde{s}_k\left(\mathbf{f}\frac{z-h}{z}\right). \tag{A10}
$$

Inserting (A9) into (A8) and solving for $\tilde{g}_k(\mathbf{f})$ yields

$$
\tilde{\mathbf{g}}^{s*}(\mathbf{f},h) = \left[\mathbf{A}^s\left(\mathbf{f}\frac{z-h}{z}\right)+\mathbf{v}'\left(\mathbf{f}\frac{z-h}{z}\right)\right]^{-1}\mathbf{c}^s(\mathbf{f},h) \tag{A11}
$$

where

$$
\begin{aligned}
c_k^s(\mathbf{f},h) &= (z/(z-h))^{-11/3}C_n^2(h)\exp(-2\pi i\mathbf{f}\cdot\boldsymbol{\theta}_k h)\ /c_0 \\
a_{kk'}^s(\mathbf{f}) &= \int_0^z (z/(z-h'))^{-5/3}C_n^2(h')\exp(2\pi i\mathbf{f}\cdot(\boldsymbol{\theta}_{k'}-\boldsymbol{\theta}_k)h')\mathrm{d}h'\ /c_0 \\
v'_{kk'}(\mathbf{f}) &= v_k^2(\mathbf{f})\delta_{kk'}/\left(9.69\times10^{-3}f^{-11/3}c_0\right)
\end{aligned}
\tag{A12}
$$

To calculate the mean square wavefront error, we substitute the expression for the optimal index estimate (A10) into (25) and use (23)

$$\tilde{\varepsilon}(\mathbf{f},\boldsymbol{\theta}) = \frac{2\pi}{\lambda}\int_0^z \left[\delta\tilde{n}(\mathbf{f},h) - \sum_k \tilde{g}_k(\mathbf{f},h) \right.$$
$$\left. \times\left(\int_0^z \left(\frac{z}{z-h'}\right)^2 \delta\tilde{n}\left(\mathbf{f}\frac{z-h}{z-h'},h'\right)\exp\left(-2\pi i\mathbf{f}\cdot\boldsymbol{\theta}_k\frac{z-h}{z-h'}h'\right)\mathrm{d}h' + \frac{\lambda}{2\pi}v_k\left(\mathbf{f}\frac{z-h}{z}\right)\right)\right]$$
$$\times\exp(-2\pi i\mathbf{f}\cdot\boldsymbol{\theta}h)\mathrm{d}h \qquad \text{(A13)}$$

Taking the expected square and using the delta-correlation property of index with altitude we get an expression for the squared error variance:

$$\left\langle\tilde{\varepsilon}^2(\mathbf{f},\boldsymbol{\theta})\right\rangle = \left(\frac{2\pi}{\lambda}\right)^2\int_0^z W_{\delta n}(\mathbf{f},h)\mathrm{d}h - \int_0^z\int_0^z \sum_k \tilde{g}_k(\mathbf{f},h)$$
$$\times\left(\frac{z}{z-h'}\right)^2 W_{\delta n}\left(\mathbf{f}\frac{z-h}{z-h'},h'\right)\exp\left(-2\pi i\mathbf{f}\cdot\boldsymbol{\theta}_k\frac{z-h}{z-h'}h'\right) \qquad \text{(A14a)}$$
$$\times\exp(-2\pi i\mathbf{f}\cdot\boldsymbol{\theta}h)\exp(2\pi i\mathbf{f}\cdot\boldsymbol{\theta}h')\mathrm{d}h\mathrm{d}h'$$
$$+\int_0^z\sum_k|\tilde{g}_k(\mathbf{f},h)|^2 v_k^2\left(\mathbf{f}\frac{z-h}{z}\right)\mathrm{d}h$$

or

$$\left\langle\tilde{\varepsilon}^2(\mathbf{f},\boldsymbol{\theta})\right\rangle = c_0 W_0(f)\left[1 - \int_0^z\int_0^z \sum_k \tilde{g}_k(\mathbf{f},h)\right.$$
$$\times\left(\frac{z}{z-h'}\right)^2\left(\frac{z-h}{z-h'}\right)^{-11/3} C_n^2(h')\exp\left(-2\pi i\mathbf{f}\cdot\boldsymbol{\theta}_k\frac{z-h}{z-h'}h'\right) \qquad \text{(A14b)}$$
$$\times\exp(-2\pi i\mathbf{f}\cdot\boldsymbol{\theta}h)\exp(2\pi i\mathbf{f}\cdot\boldsymbol{\theta}h')\mathrm{d}h\mathrm{d}h' \;/c_0$$
$$\left.+\int_0^z\sum_k|\tilde{g}_k(\mathbf{f},h)|^2 v_k'\left(\mathbf{f}\frac{z-h}{z}\right)\mathrm{d}h\right]$$

The above expression is difficult (but not necessarily impossible) to compute numerically because of the nested double integration over altitude. An interesting approximation to explore is to assume that *z*>>*h*, and set all the (*z*-*h*)/(*z*-*h'*) factors to one. In that case, the double integral separates out, and the expression for residual error variance becomes

$$\left\langle\tilde{\varepsilon}^2(\mathbf{f},\boldsymbol{\theta})\right\rangle \cong c_0 W_0\left[1 - \sum_k \bar{g}_k(\mathbf{f},\boldsymbol{\theta})\bar{c}_k(\mathbf{f},\boldsymbol{\theta}) + \int_0^z\sum_k|\tilde{g}_k(\mathbf{f},h)|^2 v_k'\left(\mathbf{f}\frac{z-h}{z}\right)\mathrm{d}h\right] \qquad \text{(A15)}$$

which can more easily be computed. We have defined $\bar{g}_k(\mathbf{f},\boldsymbol{\theta}) = \int_0^z \tilde{g}_k(\mathbf{f},h)\exp(-2\pi i\mathbf{f}\cdot\boldsymbol{\theta}h)\mathrm{d}h$ and

$$\begin{aligned}\bar{c}_k(\mathbf{f},\boldsymbol{\theta}) &= \int_0^z \left(z/(z-h)\right)^2 c_k^s(\mathbf{f},h)\exp(2\pi i\mathbf{f}\cdot\boldsymbol{\theta}h)\mathrm{d}h \\ &= \int_0^z \left(z/(z-h)\right)^{-5/3} C_n^2(h)\exp(2\pi i\mathbf{f}\cdot(\boldsymbol{\theta}-\boldsymbol{\theta}_k)h)\mathrm{d}h \quad /c_0\end{aligned} \tag{A16}$$

Equation (A15) is has a resemblance to, but is not the same as, the expression for residual variance in the plane wave case. The difference is that in the spherical wave solution, the filters *a* and *c* contain lateral stretching factors.

ACKNOWLEDGEMENTS

The author would like to thank Brent Ellerbroek of the National Optical Astronomy Observatories New Initiatives Office for running comparison simulations using his MCAO simulator code LAOS/TAOS.

This work was supported in part by the National Science Foundation Science and Technology Center for Adaptive Optics, managed by the University of California at Santa Cruz under cooperative agreement No. AST-9876783.

REFERENCES

1. Ellerbroek, B., *Efficient computation of minimum-variance wave-front reconstructors with sparse matrix techniques*, JOSA-A, 19, 9, Sept. 2002, pp 1803-1816.

2. Tokovinin, A., Viard, E., *Limiting precision tomographic phase estimation*, JOSA-A, 18, 4, Apr. 2001, pp873-882.

3. Wallner, E.P., *Optimal wave-front correction using slope measurements*, JOSA-A, 73, Dec. 1983, pp 1771-1776.

4. Gavel, D., Wiberg, D., *Toward Strehl-optimizing adaptive optics controllers*, Proc. SPIE, 4839, Feb. 2003, pp. 890-901.

5. Tokovinin, A., Le Louarn, M., Sarazin, M., *Isoplanatism in a multiconjugate adaptive optics system*, JOSA-A, 17, 10, Oct. 2000, pp1819-1827.

6. Hardy, J. W., *Adaptive optics for astronomical telescopes*, New York, NY: Oxford University Press, 1998.

7. Poyneer, L., Gavel, D., and Brase, J., *Fast wave-front reconstruction in large adaptive optics systems with use of the Fourier transform*, JOSA-A, 19, 10, October, 2002, pp2100-2111.

8. Le Roux, B., Conan, J.-M., Kulcsar, C., Raynaud, H.-F., Mugnier, Laurent M., Fusco, T., *Optimal control law for multiconjugate adaptive optics*, Proc. SPIE, 4839, Feb 2003, pp. 878-889.

9. Ellerbroek, B., Vogel, C., *Simulations of closed-loop wavefront reconstruction for multiconjugate adaptive optics on giant telescope*, Proc. SPIE, 5169, Feb. 2003, pp. 206-217.

10. Noll, R. J., *Zernike polynomials and atmospheric turbulence*, JOSA, 66, Mar. 1976, p. 207-211.